Nano Research
DOI 10.1007/s12274-014-0476-1
Research Article

ISSN 1998-0124
CN 11-5974/O4

Selective and localized laser-anneal effect for high-performance flexible multilayer MoS_2 thin-film transistors

Hyuk-Jun Kwon[1,†], Woong Choi[2,†], Daeho Lee[1,3], Yunsung Lee[4], Junyeon Kwon[4], Byungwook Yoo[5], Costas P. Grigoropoulos[1] (✉), and Sunkook Kim[4] (✉)

Nano Res., **Just Accepted Manuscript** • DOI: 10.1007/s12274-014-0476-1
http://www.thenanoresearch.com on April 15, 2014

© Tsinghua University Press 2014

Just Accepted

This is a "Just Accepted" manuscript, which has been examined by the peer-review process and has been accepted for publication. A "Just Accepted" manuscript is published online shortly after its acceptance, which is prior to technical editing and formatting and author proofing. Tsinghua University Press (TUP) provides "Just Accepted" as an optional and free service which allows authors to make their results available to the research community as soon as possible after acceptance. After a manuscript has been technically edited and formatted, it will be removed from the "Just Accepted" Web site and published as an ASAP article. Please note that technical editing may introduce minor changes to the manuscript text and/or graphics which may affect the content, and all legal disclaimers that apply to the journal pertain. In no event shall TUP be held responsible for errors or consequences arising from the use of any information contained in these "Just Accepted" manuscripts. To cite this manuscript please use its Digital Object Identifier (DOI®), which is identical for all formats of publication.

TABLE OF CONTENTS (TOC)

Selective and localized laser-anneal effect for high-performance flexible multilayer MoS_2 thin-film transistors

Hyuk-Jun Kwon[1,†], Woong Choi[2,†], Daeho Lee[1,3], Yunsung Lee[4], Junyeon Kwon[4], Byungwook Yoo[5], Costas P. Grigoropoulos[1,*], and Sunkook Kim[4,*]

[1]Department of Mechanical Engineering, University of California, Berkeley, CA 94720, USA
[2]School of Advanced Materials Engineering, Kookmin University, Seoul 136-702, South Korea
[3]Department of Mechanical Engineering, Gachon University, Seongnam-si, Gyeonggi 461-701, South Korea
[4]Department of Electronics and Radio Engineering, Kyung Hee University, Gyeonggi 446-701, South Korea
[5]Flexible Display Research Center, Korea Electronics Technology Institute, Seongnam, Gyeonggi 463-816, South Korea
[†] These authors contributed equally to this publication.

Page Numbers. The font is ArialMT 16 (automatically inserted by the publisher)

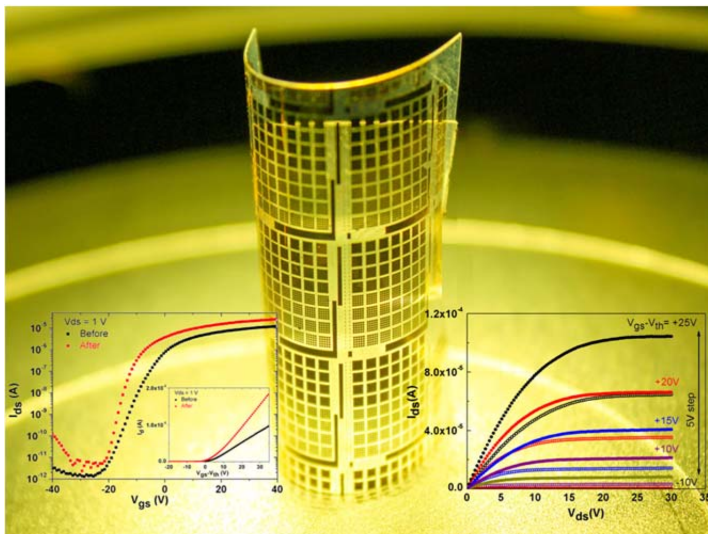

Flexible multilayer MoS_2 field effect transistors (FETs) enhanced by ultra-short pulsed laser anneal process are demonstrated without inflicted thermal damage. The reduced contact resistance after laser annealing provided significant improventment in transistor performance including higher peak field-effect mobility, increased output resistance, increased self-gain, and decreased subthreshold swing.

Nano Res
DOI (automatically inserted by the publisher)
Research Article

Selective and localized laser-anneal effect for high-performance flexible multilayer MoS_2 thin-film transistors

Hyuk-Jun Kwon[1,†], Woong Choi[2,†], Daeho Lee[1,3], Yunsung Lee[4], Junyeon Kwon[4], Byungwook Yoo[5], Costas P. Grigoropoulos[1] (✉), and Sunkook Kim[4] (✉)

[1] Department of Mechanical Engineering, University of California, Berkeley, CA 94720, USA
[2] School of Advanced Materials Engineering, Kookmin University, Seoul 136-702, South Korea
[3] Department of Mechanical Engineering, Gachon University, Seongnam-si, Gyeonggi 461-701, South Korea
[4] Department of Electronics and Radio Engineering, Kyung Hee University, Gyeonggi 446-701, South Korea
[5] Flexible Display Research Center, Korea Electronics Technology Institute, Seongnam, Gyeonggi 463-816, South Korea
[†] These authors contributed equally to this publication.

Received: day month year / Revised: day month year / Accepted: day month year (automatically inserted by the publisher)
© Tsinghua University Press and Springer-Verlag Berlin Heidelberg 2013

ABSTRACT

We report enhanced performance of multilayer MoS_2 field effect transistors (FETs) on flexible plastic substrates with ultra-short, pulsed-laser annealed Ti/Au contacts without thermal damage. An analysis of the temperature distribution, based on finite difference methods, enabled understanding of the compatibility of our picosecond laser annealing for flexible PEN substrate with low thermal budget (< 200°C). The reduced contact resistance after laser annealing provided significant improvement in transistor performance including higher peak field-effect mobility (from 24.84 $cm^2V^{-1}s^{-1}$ to 44.84 $cm^2V^{-1}s^{-1}$), increased output resistance (0.42 MΩ at V_{gs}-V_{th}= 20 V, three times higher), 6-fold increase of the self-gain, and decreased subthreshold swing. Transmission electron microscopy analysis and current-voltage measurements suggested that the reduced contact resistance is resulted from the decrease of Schottky barrier width at the MoS_2-metal junction. These results demonstrate that the selective contact laser annealing is an attractive technology for fabricating low-resistivity metal-semiconductor junctions, providing important implications for the application of high-performance two-dimensional semiconductor FETs toward flexible electronics.

KEYWORDS

Transition metal dichalcogenides, MoS_2, laser annealing, thin-film transistors, flexible electronics

1 Introduction

The development of mechanically flexible/stretchable electronics has attracted significant interest due to their potential applications. Possible uses include lightweight, portable, and conformable products such as flexible OLED displays [1], solar cells and batteries [2], wearable health patches for personal

Address correspondence to Costas P. Grigoropoulos, cgrigoro@me.berkeley.edu; Sunkook Kim, seonkuk@hku.ac.kr

health monitoring/therapeutics and implantable medical devices [3,4]. Advances in materials research, including development of flexible substrates, stretchable metal interconnects, and low-temperature process (< 100°C), have resulted in substantial progress in bendable and conformal thin-film transistors (TFTs). In spite of the many capabilities of conventional TFTs based on amorphous silicon (a-Si), low temperature poly-silicon (LTPS), organic semiconductors, and oxide semiconductors, the fragile nature and low mobility of these materials limit their utility in flexible/stretchable electronic circuits. Hence, the reliable performance of TFT-based devices requires a novel semiconductor material that can provide mechanical stability and high mobility.

Recently, two-dimensional (2D) layered semiconductors (series of transition metal dichalcogenides (TMDs) with the formula of MX_2 (M = Mo, W; X = S, Se, Te)) have the potential to overcome the drawbacks of conventional TFTs, because of the exotic electrical and mechanical properties of 2D crystals [5]. Among the layered semiconductors which are composed of vertically stacked layers held together by van der Waals interactions, molybdenum disulfide (MoS_2) is drawing attention as a promising alternative to large area silicon-thin-film-based electronics. Single or multilayer MoS_2 exhibits intriguing characteristics: relatively large bandgap (1.2 - 1.9 eV), high mobility at room temperature (up to ~100 $cm^2\ V^{-1}s^{-1}$), low subthreshold swing (SS ~70 mV $decade^{-1}$), and an absence of dangling bonds [6-8]. However, high performance MoS_2 TFTs require the formation of low-resistivity metal-MoS_2 junctions since the presence of Schottky barriers has been reported between typical Ti/Au contacts and MoS_2 [9-11]. Non-ideal electric contacts formed on MoS_2 can fundamentally hamper any attempts to improve transistor performance.

In order to reduce contact resistivity between metal electrodes and MoS_2, the use of thermal annealing [8], highly-doped interface [12], or scandium electrodes [13] to date has been suggested. However, conventional high-temperature thermal processes are not compatible with commonly used flexible substrates (e.g., PEN, PET, and PI) because of their low thermal budget (< 200°C). Since conventional thermal annealing affects the entire wafer, heat can also damage to the components or sensitive parts where thermal effects should be avoided. In addition, the doping stability of highly-doped interface significantly limits commercial feasibility since the chemical doping effect decreases gradually over time. Furthermore, scandium metals have little commercial appeal because of their low availability and the difficulties in the preparation of metallic scandium.

Laser annealing is an alternative method of achieving low contact resistivity. Pulsed laser annealing had previously been used for mitigating the lattice damage caused by ion implantation of dopant atoms in semiconductors [14-16]. However, in these earlier studies, laser annealing technique had been only applied to rigid applications and to conventional semiconducting materials (Si and Ge). In this paper, we for the time investigate the effects of selective annealing of Ti/Au metal contacts in MoS_2 transistors on plastic substrates using picosecond ultra-fast pulsed laser with high-repetition rate (80 MHz). Since the irradiation of pulsed lasers onto metal raises the temperature of a confined area, this method can achieve thermal annealing effect without thermal damage. Moreover, the selective contact annealing improves performance metrics of flexible MoS_2 TFTs such as higher peak field-effect mobility of 44.84 $cm^2\ V^{-1}s^{-1}$, improved current saturation, and decreased SS due to reduced contact resistance. Based on transmission electron microscopy (TEM) analysis and current-voltage measurements, we suggest that the reduced contact resistance is resulted from the decreased Schottky barrier width. Furthermore, the numerically predicted temperature field indicates that a high annealing temperature can be obtained with our ultra-fast picosecond laser system without thermal damage of flexible substrates, which is a key feature for reducing the Schottky barrier width. These results demonstrate that further improvement of contact resistivity is possible with the laser annealing of metal contacts without substrate deformation, providing important implications for the realization of high-performance flexible TFTs based on TMDs.

2 Results and discussion

2.1 Flexible MoS_2 transistors and laser annealing system

Fig. 1(a) and 1(b) show our proof-of-concept bottom-gated MoS_2 TFTs on a flexible DuPont PEN substrate. The fabrication begins with the ion-assisted deposition (IAD) of a 100-nm-thick indium thin oxide (ITO) bottom electrode on a plastic substrate at room temperature. Subsequently, stacked gate dielectrics are composed of an atomic-layer-deposited (ALD) Al_2O_3 film (50 nm) and a sputter-deposited SiO_2 layer (250 nm). Next, multilayer MoS_2 flakes are mechanically exfoliated from bulk MoS_2 crystals (SPI Supplies, USA) and transferred to the deposited stack gate dielectrics. Atomic force microscopy (AFM) measurements

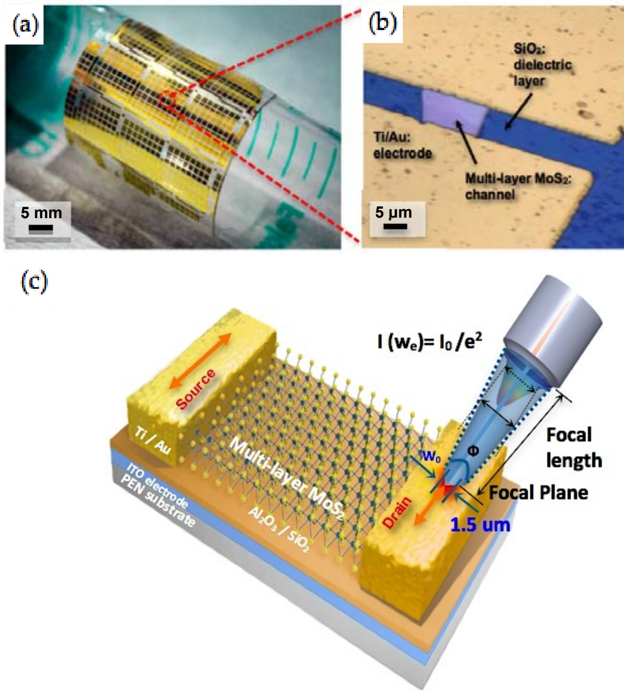

Figure 1 Bottom-gated MoS_2 transistors on flexible substrates and pulsed laser annealing system. (a) Photograph of flexible multilayer MoS_2 transistors on a plastic substrate showing mechanical flexibility. (b) The 3D confocal laser microscope image of multilayer MoS_2 transistors with ALD Al_2O_3 / SiO_2 gate dielectric on the flexible PEN substrate. (c) Gaussian beam intensity distribution and its shape near the focal plane. $2W_0$ is the beam waist, Φ is the beam divergence angle, and 1.5 μm beam diameter based on the $1/e^2$ intensity. The picosecond laser irradiation with a Gaussian beam profile is focused and scanned along the edge of the source and drain electrodes.

show the thickness of MoS_2 channels is in the range of 30-80 nm. For the formation of the well-established contacts with MoS_2 semiconducting material, Ti was selected among the low work function materials because the favorable interface geometry of Ti allows bonding and the electronic density of states (DOS) at the Fermi level to maximize through increasing the overlap between states at the interface [7]. Strong interconnections result in narrow and low potential barriers to maximize current injection. Ti (10 nm) and Au (300 nm) layers as source and drain electrode contacts are patterned by conventional photolithography and lift-off technique and deposited by electron-beam evaporation at room temperature. After device fabrication, the electrode contact region with MoS_2 is irradiated using a commercial neodymium-doped yttrium vanadate ($Nd:YVO_4$) picosecond pulsed laser from Newport (wavelength: 355 nm, pulse width based on full width at half maximum: 12 ps, pulse repetition rate: 80 MHz) as shown in Fig. 1(c). The laser beam is focused on the edge of the contacts as charge injection across contacts between bulk and thin-film materials usually occurs from the contact edge [17]. The irradiated laser with short wavelength of the laser beam (355 nm) is efficiently absorbed at Au electrode [18]. The focused laser beam has a Gaussian beam shape of 1.5 μm diameter at $1/e^2$ of peak irradiance along the propagation direction. The Gaussian laser-beam intensity within the focal plane has the form, $I(r) = I_0 exp(-2r^2/w_e^2)$, where w_e is the radius of the laser focus defined by $I(w_e) = I_0/e^2$, $w_e = \sqrt{2}w_0$. The target sample was placed on a high-resolution x-y positioning stage (Aerotech).

2.2 Numerical analysis for temperature distribution during laser annealing process

We investigate temperature distribution during laser annealing by numerical analysis. Fig. 2(a) and 2(b) show the results calculated by 3-dimensional (3D) finite-difference methods (FDM) using COMSOL Multiphysics for a picosecond pulsed laser source applied under our experimental conditions. We calculate the temperature distribution for average laser powers of 18.3 mW and 43.0 mW (see Supplementary Material). Fig. 2(a) shows that the generated heat is dissipated primarily to the

underlying structure by conduction with relatively minor loss to air by convection. The calculated temperatures at the top of the Au electrode labeled as "A" (at the top of Au film) and the bottom labeled as "B" (at the interface of the Au electrode and the MoS_2 channel) in Fig. 2(a) are plotted as a function of time in Fig. 2(b) (the scanning speed of laser = 10 μm s^{-1}). Because of the high repetition rate (80 MHz) of the irradiated pulses, the temperatures do not drop to the ambient temperature before the next pulse arrives [19]. This leads to heat accumulation (indicated by green regions). The elevated temperature from the heat accumulation effects was a key factor in inducing laser annealing at the location "B". The temperature distribution then consists of high-frequency and picosecond-duration spikes superposed on a continuous base (orange region at P_{avg} = 43.0 mW and blue region at P_{avg} = 18.3 mW) as shown in the inset of Fig. 2(b). The effect of the high frequency transients by an ultrashort pulsed laser lasted till the time of 0.2 sec, i.e. while location "A" is being directly irradiated by the moving Gaussian laser beam. At the moment when the center of laser beam was placed right on the middle of "A" (0.075 sec), the temperature exhibited significant variation, depending on the laser power. For the laser power of 43.0 mW, the temperature exceeded the melting point of Au (1330 K) as indicated by the orange region in Fig. 2(b). Such a high temperature may inflict thermal damage on the Au contacts. However, the induced temperature by the laser power of 18.3 mW is 533 K (blue region in Fig. 2(b)). This is a comparable temperature with those of thermal annealing used in previous studies to improve device performance [8,20,21], as well as with our experimental results detailed in subsequent sections of this paper. At this time, the Au film endured substantial temperature difference between its top and bottom surfaces, implying that the Au film helped protect the bottom of the film surface from strong sharp and high intensity irradiance. Since the position "A" was completely outside the pulsed laser beam beyond 0.2 sec, the effect of these high peaks faded due to diffusion. Therefore, the top and bottom temperatures converge and cool down completely (~ 2.6 sec.) as shown in Fig. 2(b). The valid range of laser power that allows laser processing to be compatible with plastic substrates

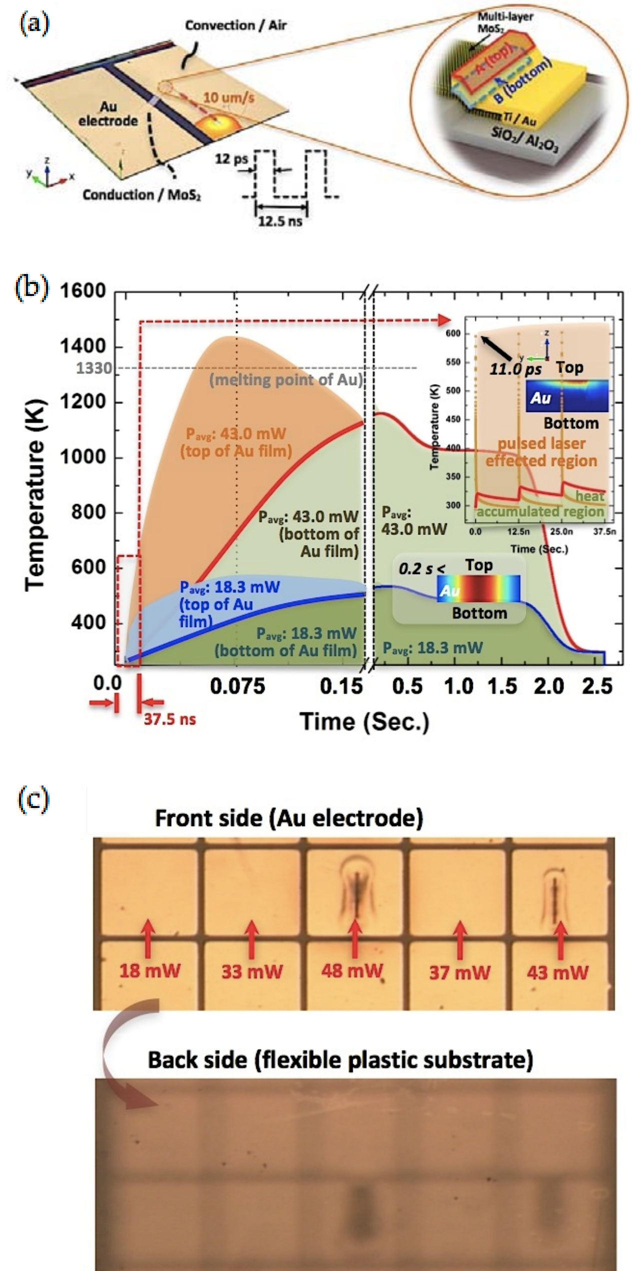

Figure 2 Numerical results calculated by Finite Difference Methods for the temperature distribution under picosecond-pulsed laser source. (a) The spatial temperature distribution along the surface when picosecond pulsed laser is applied onto the Au electrode surface in contact with air and ALD Al_2O_3 / SiO_2 dielectric layer. (b) The temperature of Au electrode versus exposure time at the specific points "A" (the top of Au film) and "B" (the interface of the Au electrode and the MoS_2 channel) in (a) irradiated by the center of the laser beam. The 37.5 ns window (not on scale in the horizontal time axis) is depicted in the insert. (c) The optical images of the front and back side of laser-irradiated Au contacts on a flexible plastic substrate. Au contacts irradiated with laser power > 40 mW show severe damage.

can be tested by irradiating laser beams on the Au contacts. Fig. 2(c) shows the optical images of laser-irradiated Au contacts on plastic substrate. In agreement with the numerical analysis, the laser with its power > 40 mW severely damages the Au electrode.

2.3 Effects of laser annealing

To investigate the effect of laser annealing on the contact resistance of MoS_2 transistors, we first fabricate MoS_2 TFTs on SiO_2 (250 nm) / p^+-Si wafers and measure the source-drain current and voltage (I_{ds}-V_{ds}) characteristics as two-terminal devices (gate is not biased) before and after laser annealing. Fig. 3(a) clearly shows the steeper slope after laser annealing (laser power of 18.3 mW and scan speed of 10 μm s^{-1}), indicating an improved contact behavior. To see the effect of laser power on the contact resistance, the changes in contact resistance per width (R_CW; R_C: contact resistance, W: width of the contact) after laser annealing are calculated based on the model shown in Fig. 3(b). The total resistance R between source and drain of the MoS_2 transistor is given by [22]:

$$R = R_S \frac{d}{W} + 2R_C, \quad (1)$$

where R_S is MoS_2 sheet resistance and d is the distance between contacts. If the change in R_S is negligible after laser annealing, the change in resistance is given by:

$$\Delta R = R_{After} - R_{Before} = 2\Delta R_C. \quad (2)$$

We then can calculate ΔR_CW (= $\Delta RW/2$) based on the estimated parameters from Fig. 3(a) (ΔR) and optical images (W). Among five different laser powers between 5 mW and 40 mW, the normalized ΔR_CW in Fig. 3(c) shows that 18.3 mW provides the greatest reduction in R_CW. If the laser power is too low, the laser irradiation does not increase the temperature enough to affect the contact behavior. On the other hand, if the laser power is too high, the annealing temperature becomes so high that it possibly starts the deterioration of the contact behavior. It needs to be mentioned that the R_CW values of MoS_2-metal contacts reported in literature scatter in the range of 3.3-80 Ω·mm [21,23-25]. Although we could not obtain an absolute value of R_CW within the given experimental conditions, a consistent reduction of contact resistance in various MoS_2 transistors after laser annealing at 18.3 mW demonstrates the

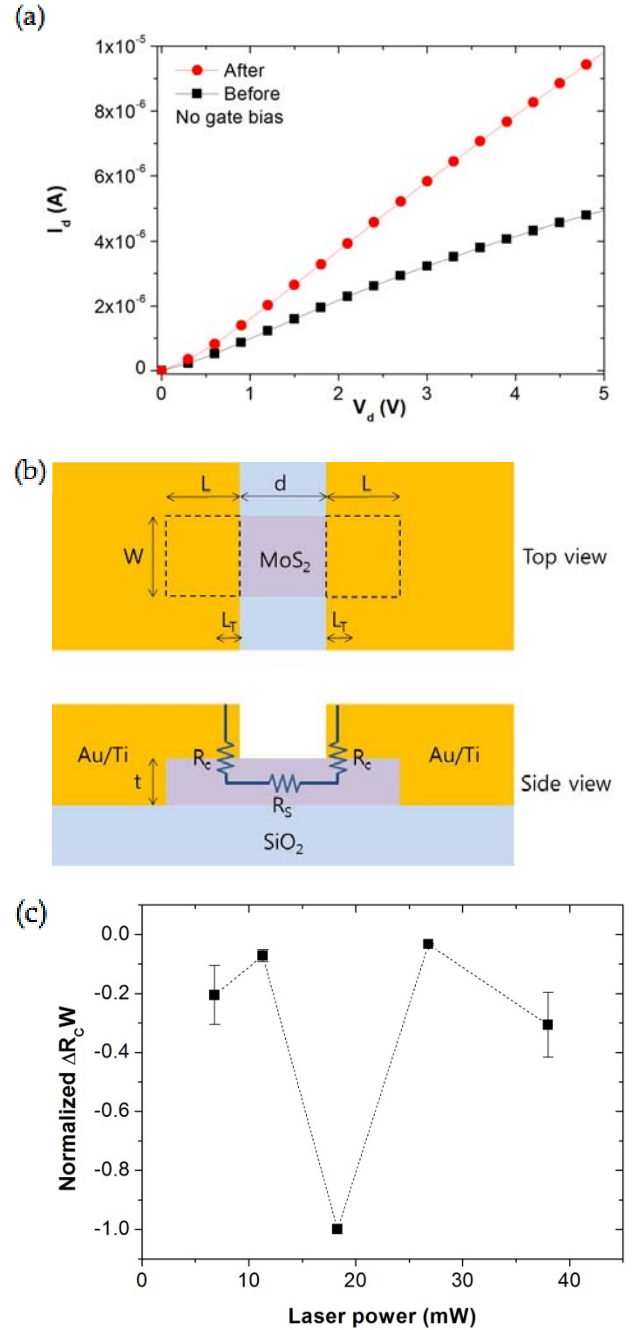

Figure 3 Effects of laser annealing on the contact resistivity of multilayer MoS_2 transistors fabricated on Si wafers. (a) The I_{ds}-V_{ds} characteristics of MoS_2 transistors at V_g = 0 V before and after laser annealing. The slope is steeper after laser annealing, indicating an improved contact behavior. (b) Schematic device configuration with an equivalent circuit model. (c) The reduction of contact resistance per width after laser annealing normalized with respect to that of 18.8 mW ($\Delta R_cW = (R_cW)_{After}-(R_cW)_{Before}$). V_{ds} = 1 V and scan speed = 10 μm s^{-1}.

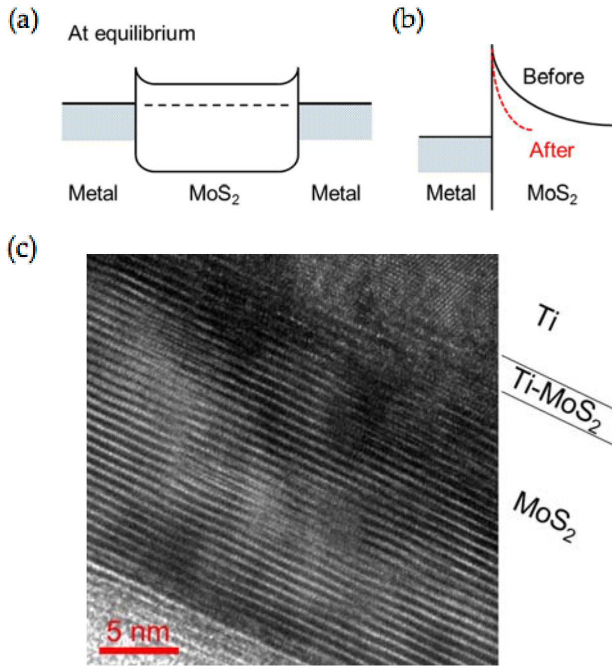

Figure 4 Effect of laser annealing on metal-MoS_2 junction after laser annealing. (a) Schematic energy-band diagrams of a multilayer MoS_2 transistors with a Schottky barrier at equilibrium. (b) Schematic band diagram of the metal-MoS_2 junction illustrating the reduction of the Schottky barrier width after laser annealing. (c) A cross-sectional TEM image showing the diffusion of Ti into MoS_2 at the interface after laser annealing.

robustness and reproducibility of this method.

Fig. 4(a) shows the schematic energy band diagram for the MoS_2 transistor in thermal equilibrium. If we assume the existence of a Schottky barrier between metal contacts and a semiconductor, thermionic emission and/or tunneling will allow electron transport during transistor operation. According to Das *et al.*, thermionic emission and tunneling though Schottky barrier limit the charge injection during off- and on-state of MoS_2 transistors, respectively [13]. The dominant mechanism that reduced contact resistance in Fig. 3 is not clear as the gate was floated during the measurement of source-drain current. However, the significant increase of the on-current after laser annealing in Fig. 5 suggests that laser annealing increases the tunneling current across the Schottky barrier. Since the tunneling current will exponentially increase with $N_D^{0.5}$, where N_D is carrier concentration [26], the decreased contact resistance after laser annealing is probably due to the reduced tunneling barrier width, which is resulted from the increased carrier concentration at the interface.

This explanation is supported by the cross-sectional TEM image shown in Fig. 4(c). Along the interface between Ti and MoS_2, diffusion of Ti into MoS_2 can be observed after laser annealing. This observation is consistent with the reports that Ti forms a solid solution with MoS_2 by placing Ti atoms between the neighboring S planes of MoS_2 and that thermal annealing at 300°C induces solid-state diffusion in Ti thin film [27,28]. As Ti-doped MoS_2 becomes more conductive due to increased n-type doping [29], the reduction of tunneling barrier width by the formation of a Ti-MoS_2 solid solution at the interface is thought to be the dominant mechanism of the decreased contact resistance after laser annealing.

We then investigated the effect of laser annealing on device performance of MoS_2 TFTs on flexible PEN substrates. The thickness of the MoS_2 flake of our representative device (t_{ch}) is ~50 nm, and the back gate oxide thickness (t_{ox}) is ~300 nm (SiO_2 (250 nm) and Al_2O_3 (50 nm)). Fig. 5(a) shows the log- and linear-scale drain current vs. gate-source voltage (I_{ds}-V_{gs}) characteristics for the same MoS_2 TFTs, measured before (black circles) and after laser annealing (red circles) with a power of 18.3 mW. Following selective laser annealing on contacts in MoS_2 TFTs, transistor performance metrics, including on/off-current ratio (I_{on}/I_{off}), peak field-effect mobility (μ_{eff}), subthreshold swing (SS), output resistance (R_o), and voltage-gain for transistor (A_v), were improved. As shown in Fig. 5(a), the I_{on}/I_{off} after laser annealing was observed as > 10^6 without a change in I_{off}. The peak field-effect mobility ($\mu_{eff} = Lg_m/(WC_{ox}V_{ds})$) extracted from Fig. 5(a) increased almost two-fold after laser annealing (from 24.84 $cm^2 V^{-1}s^{-1}$ to 44.84 $cm^2 V^{-1}s^{-1}$). Here, L, g_m, W, C_{ox} are channel length (L = 7 μm), transconductance, channel width (W = 7.75 μm), and oxide capacitance, respectively. The value of μ_{eff} observed in our MoS_2 TFTs exceeds those reported in previous MoS_2 TFTs on flexible substrates (4.7-24 $cm^2 V^{-1}s^{-1}$) [25,30,31] as well as in organic TFTs or a-Si TFTs on flexible plastic substrates (< 1 $cm^2 V^{-1}s^{-1}$). Statistically, μ_{eff} of the tested MoS_2 TFTs increased from ~15±10 $cm^2 V^{-1}s^{-1}$ to ~35±10 $cm^2 V^{-1}s^{-1}$ after laser annealing. No dependence on channel thickness was observed

within the given experimental conditions. Fig. 5(b) shows the drain current as a function of the drain voltage (I_{ds}-V_{ds}) before (open circles) and after laser annealing (solid circles). At the same V_{gs}-V_{th}, the laser annealing results in ohmic behavior in linear regime and higher current saturation. Following laser annealing, R_o significantly increased to 0.42 MΩ at V_{gs}-V_{th}= 20 V, which is three times higher than values for as-fabricated devices. The most prominent effect of laser annealing is the self-gain ($A_v = g_m R_o$) in MoS_2 TFTs, which exhibits six-fold increase due to enhancement of g_m and R_o. These results have an especially important technological implication for

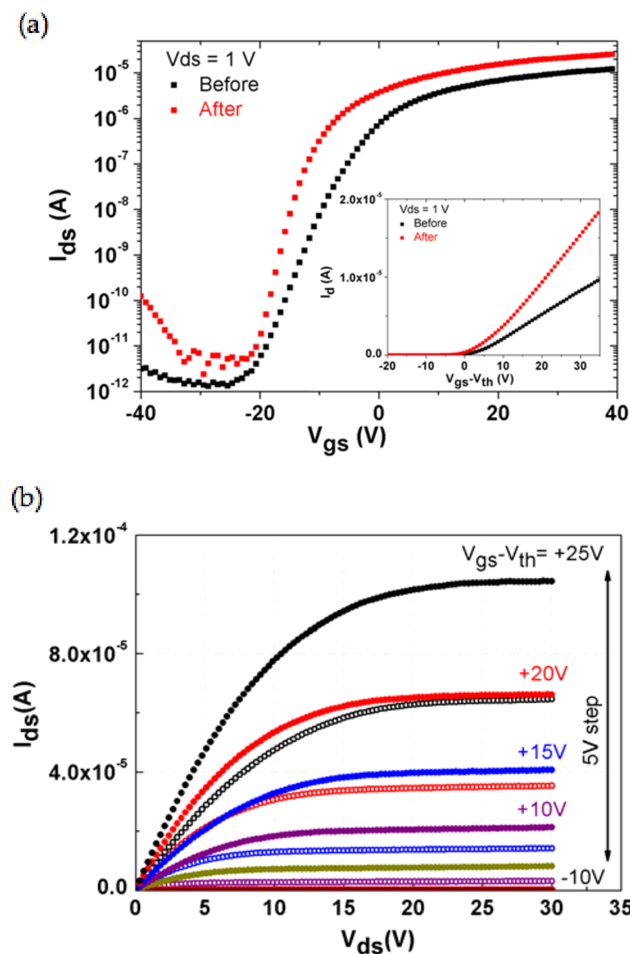

Figure 5 The enhanced performance of a representative flexible MoS_2 transistor by the selective laser-annealing of contacts. (a) The log-scale I_{ds}-V_{gs} characteristics for a MoS_2 transistor (L = 7 μm) before and after laser annealing at V_{ds} = 1 V. Inset shows the I_{ds}-(V_{gs}-V_{th}) in linear-scale. The V_{th} of as-fabricated device is -2.1V, but V_{th} is shifted to -7.2V after laser annealing. (b) The I_{ds}-V_{ds} characteristics of the MoS_2 transistor before (open circle) and after (solid circle) laser annealing. V_{gs}-V_{th} ranges from -10 to 25 V in 5 V steps.

electronic amplifiers used to increase the power of a signal in flexible/stretchable electronics.

3 Conclusions

In summary, selective annealing of source/drain electrodes in MoS_2 TFTs on mechanically flexible substrates by picosecond laser achieved enhanced device performance without damaging plastic substrates. An analysis of the temperature distribution, based on finite difference methods, exhibited the compatibility of our picosecond laser annealing with the flexible substrate. Flexible MoS_2 TFTs with laser-annealed contacts are especially promising for use in low-power operation (low subthreshold slope), high-speed devices (higher mobility), and the amplification of self-gain (the fully saturated drain current). Analysis with FDM simulation, I-V characteristics, and TEM observation strongly suggest that the significant enhancement in performance metrics originate from a decrease of Schottky barrier width between Ti/Au metal and the semiconducting MoS_2. These results demonstrate that picosecond laser annealing is an attractive technology for realizing high performance flexible MoS_2 TFTs in analog/digital integrated circuits.

Acknowledgements

This research was supported by the National Research Foundation of Korea (NRF-2013K1A3A1A32035549), a grant (KHU-20121643) from Kyung Hee University, and the Industrial Strategic Technology Development Program (10045145). H.-J. Kwon, D. Lee, and C. P. Grigoropoulos gratefully acknowledge the US Air Force Office of Scientific Research AFOSR/AOARD under Grant FA2386-13-4123. W. Choi acknowledges the financial support of the New Faculty Research Program 2012 of Kookmin University in Korea and the National Research Foundation of Korea (NRF-2013R1A1A2008191).

Electronic Supplementary Material: Supplementary material (computational detail of ultrafast electron dynamics and temperature distribution through 3D FDM) is available in the online version of this article at http://dx.doi.org/10.1007/s12274-***-****-* (automatically inserted by the publisher).

References

[1] Kim, S.; Kwon, H. J.; Lee, S.; Shim, H.; Chun, Y.; Choi, W.; Kwack, J.; Han, D.; Song, M.; Kim, S.; Mohammadi, S.; Kee, I.; Lee, S. Y. Low-power flexible organic light-emitting diode display device. *Adv. Mater.* **2011**, *23*, 3511-3516.

[2] Kuang, D.; Brillet, J.; Chen, P.; Takata, M.; Uchida, S.; Miura, H.; Sumioka, K.; Zakeeruddin, S. M.; Gratzel, M. Application of highly ordered TiO_2 nanotube arrays in flexible dye-sensitized solar cells. *Acs Nano* **2008**, *2*, 1113-1116.

[3] Kim, D. H.; Lu, N.; Ma, R.; Kim, Y. S.; Kim, R. H.; Wang, S.; Wu, J.; Won, S. M.; Tao, H.; Islam, A.; Yu, K. J.; Kim, T. I.; Chowdhury, R.; Ying, M.; Xu, L.; Li, M.; Chung, H. J.; Keum, H.; McCormick, M.; Liu, P.; Zhang, Y. W.; Omenetto, F. G.; Huang, Y.; Coleman, T.; Rogers, J. A. Epidermal electronics. *Science* **2011**, *333*, 838-843.

[4] Viventi, J.; Kim, D. H.; Moss, J. D.; Kim, Y. S.; Blanco, J. A.; Annetta, N.; Hicks, A.; Xiao, J. L.; Huang, Y. G.; Callans, D. J.; Rogers, J. A.; Litt, B. A Conformal, bio-interfaced class of silicon electronics for mapping cardiac electrophysiology. *Sci. Transl. Med.* **2010**, *2*, 24ra22.

[5] Wang, Q. H.; Kalantar-Zadeh, K.; Kis, A.; Coleman, J. N.; Strano, M. S. Electronics and optoelectronics of two-dimensional transition metal dichalcogenides. *Nat. Nanotechnol.* **2012**, *7*, 699-712.

[6] Splendiani, A.; Sun, L.; Zhang, Y. B.; Li, T. S.; Kim, J.; Chim, C. Y.; Galli, G.; Wang, F. Emerging photoluminescence in monolayer MoS_2. *Nano Lett.* **2010**, *10*, 1271-1275.

[7] Mak, K. F.; Lee, C.; Hone, J.; Shan, J.; Heinz, T. F. Atomically thin MoS_2: a new direct-gap semiconductor. *Phys. Rev. Lett.* **2010**, *105*, 136805.

[8] Radisavljevic, B.; Radenovic, A.; Brivio, J.; Giacometti, V.; Kis, A. Single-layer MoS_2 transistors. *Nat. Nanotechnol.* **2011**, *6*, 147-150.

[9] Yoon, Y.; Ganapathi, K.; Salahuddin, S. How good can monolayer MoS_2 transistors be? *Nano Lett.* **2011**, *11*, 3768-3773.

[10] Popov, I.; Seifert, G.; Tomanek, D. Designing electrical contacts to MoS_2 monolayers: a computational study. *Phys. Rev. Lett.* **2012**, *108*, 156802.

[11] Choi, W.; Cho, M. Y.; Konar, A.; Lee, J. H.; Cha, G. B.; Hong, S. C.; Kim, S.; Kim, J.; Jena, D.; Joo, J.; Kim, S. High-detectivity multilayer MoS_2 phototransistors with spectral response from ultraviolet to infrared. *Adv. Mater.* **2012**, *24*, 5832-5836.

[12] Fang, H.; Chuang, S.; Chang, T. C.; Takei, K.; Takahashi, T.; Javey, A. High-performance single layered WSe_2 p-FETs with chemically doped contacts. *Nano Lett.* **2012**, *12*, 3788-3792.

[13] Das, S.; Chen, H. Y.; Penumatcha, A. V.; Appenzeller, J. High performance multilayer MoS_2 transistors with scandium contacts. *Nano Lett.* **2013**, *13*, 100-105.

[14] Bell, A. E. Review and analysis of laser annealing, *RCA Review*, **1979**, *40*, 295-338.

[15] Wood, R. F.; Giles, G. E. Macroscopic theory of pulsed-laser annealing. 1. Thermal transport and melting, *Phys. Rev. B*, **1981**, *23,* 2923-2942.

[16] Baeri, P.; Campisano, S. U.; Foti, G.; Rimini, E. Melting model for pulsing-laser annealing of implanted semiconductors, *J. Appl. Phys.*, **1979**, *50,* 788-797.

[17] Leonard, F.; Talin, A. A. Electrical contacts to one- and two-dimensional nanomaterials. *Nat. Nanotechnol.* **2011**, *6*, 773-783.

[18] Gadenne, M.; Podolskiy, V.; Gadenne, P.; Sheng, P.; Shalaev, V. M. Plasmon-enhanced absorption by optical phonons in metal-dielectric composites. *Europhys. Lett.* **2001**, *53*, 364-370.

[19] Eaton, S. M.; Zhang, H. B.; Herman, P. R. Heat accumulation effects in femtosecond laser-written waveguides with variable repetition rate. *Opt. Express* **2005**, *13*, 4708-4716.

[20] Ishigami, M.; Chen, J. H.; Cullen, W. G.; Fuhrer, M. S.; Williams, E. D. Atomic structure of graphene on SiO_2. *Nano Lett.* **2007**, *7*, 1643-1648.

[21] Kim, S.; Konar, A.; Hwang, W. S.; Lee, J. H.; Lee, J.; Yang, J.; Jung, C.; Kim, H.; Yoo, J. B.; Choi, J. Y.; Jin, Y. W.; Lee, S. Y.; Jena, D.; Choi, W.; Kim, K. High-mobility and low-power thin-film transistors based on multilayer MoS_2 crystals. *Nat. Comm.* **2012**, *3*, 1011.

[22] Schroder, D. K. *Semiconductor Material and Device Characterization. 3rd ed.*; Wiley: New York, 2006.

[23] Liu, H.; Neal, A. T.; Ye, P. D. Channel length scaling of MoS_2 MOSFETs. *ACS Nano* **2012**, *6*, 8563-8569.

[24] Hwang, W. S.; Remskar, M.; Yan, R.; Kosel, T.; Park, J. K.; Cho, B. J.; Haensch, W.; Xing, H.; Seabaugh, A.; Jena, D. Comparative study of chemically synthesized and exfoliated multilayer MoS_2 field-effect transistors. *Appl. Phys. Lett.* **2013**, *102*, 043116.

[25] Chang, H.-Y.; Yang, S.; Lee, J.; Tao, L.; Hwang, W.-S.; Jena, D.; Lu, N.; Akinwande, D. High-performance, highly bendable MoS_2 transistors with high-k dielectrics for flexible low-power systems. *ACS Nano* **2013**, *7*, 5446-5452.

[26] Sze, S. M. *Physics of semiconductor devices. 2nd ed.*; Wiley: New York, 1981.

[27] Teer, D. G. New solid lubricant coatings. *Wear* **2001**, *251*, 1068-1074.

[28] Kitada, M.; Shimizu, N.; Shimotsu, T. Amorphous phase formation in Ti/Ni bilayer thin-films by solid-state diffusion. *J. Mater. Sci. Lett.* **1989**, *8*, 1393-1394.

[29] Kang, J.; Sarkar, D.; Liu, W.; Jena, D.; Banerjee, K. A computational study of metal-contacts to beyond-graphene 2D semiconductor materials. *IEDM Tech. Dig.,* **2012**, DOI: 10.1109/IEDM.2012.6479060.

[30] Pu, J.; Yomogida, Y.; Liu, K.-K.; Li, L.-J.; Iwasa, Y.; Takenobu, T. Highly flexible MoS_2 thin-film transistors with ion gel dielectrics. *Nano Lett.* **2012**, *12*, 4013-4017.

[31] Yoon, J.; Park, W.; Bae, G.-Y.; Kim, Y.; Jang, H. S.; Hyun, Y.; Lim, S. K.; Kahng, Y. H.; Hong, W.-K.; Lee, B. H.; Ko, H. C. Highly flexible and transparent multilayer MoS_2 transistors with graphene electrodes. *Small* **9**, *19*, 3295-3300.

Electronic Supplementary Material

Selective and localize laser-anneal effect for high-performance flexible multilayer MoS_2 thin-film transistor

Hyuk-Jun Kwon[1,†], Woong Choi[2,†], Daeho Lee[1,3], Yunsung Lee[4], Junyeon Kwon[4], Byungwook Yoo[5], Costas P. Grigoropoulos[1] (✉), and Sunkook Kim[4] (✉)

[1] Department of Mechanical Engineering, University of California, Berkeley, CA 94720, USA
[2] School of Advanced Materials Engineering, Kookmin University, Seoul 136-702, South Korea
[3] Department of Mechanical Engineering, Gachon University, Seongnam-si, Gyeonggi 461-701, South Korea
[4] Department of Electronics and Radio Engineering, Kyung Hee University, Gyeonggi 446-701, South Korea
[5] Flexible Display Research Center, Korea Electronics Technology Institute, Seongnam, Gyeonggi 463-816, South Korea
[†] These authors contributed equally to this publication.

Supporting information to DOI 10.1007/s12274-****-****-* (automatically inserted by the publisher)

1. Ultrafast electron dynamics

Profound understanding of ultrashort laser pulse induced temperature field requires detailed knowledge of the fundamental interactions between laser light (photons) and matter (electron and phonon systems). In metals, initially electrons primarily absorb the laser photon energy. In the Au film with the thickness of 400 nm, the optical absorption depth is about 16.3 nm [1]. The electron system temperature rises instantaneously in response to the applied photon flux. Thermalized hot electrons diffuse into the material and transfer their energy to the lattice (within 10^{-12} ~ 10^{-10} s) until the electron and lattice temperatures equilibrate through electron-phonon coupling. This equilibration occurs within the pulse for pulse lengths in the range 10 to 60 ps [2]. In the gold system, this thermal equilibrium time of the electron and lattice is about 40 ps [3]. Therefore, the temperatures of electron and lattice are different during the single pulse duration (12 ps) applied in our experiment. Consequently, the hot electron diffusion length is deeper than both the optical absorption depth and the heat diffusion length $\delta = \sqrt{4 \cdot \alpha \cdot dt}$ (where δ is the depth of heat penetration, α is the diffusivity of materials, and dt is the pulse duration).

In order to obtain a more accurate predictive solution, the two-temperature model (TTM) could be applied in this transient non-equilibrium case [4]. However, the TTM model that is by itself an approximation of the Boltzmann transport equation has been widely used to understand the origin of ultrashort electron dynamics under single laser pulse excitation of width 10^{-15} ~ 10^{-12} s. Prediction of the transient temperature distribution induced by high repetition rate pulsed laser over a long time scale as in our system by using the TTM poses a significant challenge due to the required prohibitively long computing time. In our 80 MHz repetition rate case, we have to compute the TTM system of equations over 80,000,000 pulses in order to analyze only one second. Although the amplitude of the ps duration temperature spikes would be smaller by the TTM model, the heat accumulation that is driven by thermal diffusion would not differ from the presented thermal model prediction. In essence, the green regions in Fig. 2 (in main manuscript) would stay the same, with the orange and blue domains representing the upper limits of the superposed temperature field envelopes.

———————————

Address correspondence to Costas P. Grigoropoulos, cgrigoro@me.berkeley.edu; Sunkook Kim, seonkuk@hku.ac.kr

2. Simulation of temperature distribution

Temperature distribution is calculated by 3-dimensional (3D) Finite-Difference Methods using COMSOL Multiphysics at a specific position when picosecond pulsed laser source is applied under our experimental condition. The equilibrium temperature approximation is adopted since it reduces the required computational cost. As previously noted, the assumption of equilibrium temperature would overestimate the transient temperature. However, the approximate thermal solution shows good agreement with the results of real laser damage test.

To calculate the approximated temperature distribution inside laser-heated Au electrode, the following heat flow equation is used:

$$\rho C_p \frac{\partial T}{\partial t} - \nabla(\mathrm{k}\nabla \mathrm{T}) = Q(x,y,z) \tag{1}$$

where ρ is the density, C_p is the specific heat, k is the thermal conductivity, and Q is the heat source term. In the volumetric heating with a Gaussian laser beam case, the heat source term is expressed as:

$$Q(x,y,z) = \mathrm{Q}_0\left(1\text{-}\mathrm{R}_c\right).\frac{A_c}{2\pi\sigma_x\sigma_y}e^{-\left[\frac{(x-x_0)^2}{2\sigma_x^2}+\frac{(y-y_0)^2}{2\sigma_y^2}\right]}.e^{-A_c z} \tag{2}$$

where Q_0 is the total input power, R_c is the reflection coefficient, A_c is the absorption coefficient, and $\sigma_{x,y}$ is pulse x,y standard deviation. Note that for the accuracy of the analysis, thermal properties of Au electrode used as absorption layer were temperature dependent thermophysical properties. However, the material properties, R_c and A_c, are assumed to be constants. In addition, the thermal properties of multilayer MoS_2 was included in this analysis by using the experimental values of previous report [5]. The top surface of Au electrode is aligned with z = 0 and the Gaussian laser beam moves over the surface at a specific speed, 10 μm s^{-1} along a prescribed path. The pulsed laser utilizes high peak power (P_{peak} = E/Δt where E is energy contained in every pulse is constant), which is calculated based on measured average power (P_{avg} = E/T = Ef) where f=1/T is repetition rate).

3. MoS_2 channel thickness

Figure S1 shows the channel thickness (~50 nm) of a representative device measured by AFM.

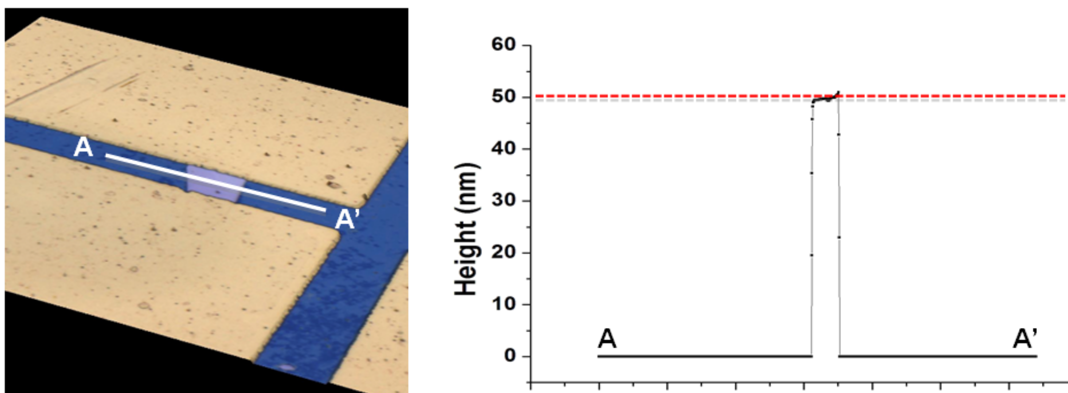

Figure S1. MoS_2 channel thickness measured by AFM.

4. TEM image before laser annealing

Due to the destructive nature of TEM characterization, it is impossible to compare the exact same interface between Ti and MoS_2 before and after laser annealing by TEM. However, the TEM images of representative devices before laser annealing did not show any evidence of Ti diffusion into MoS_2 (Figure S2).

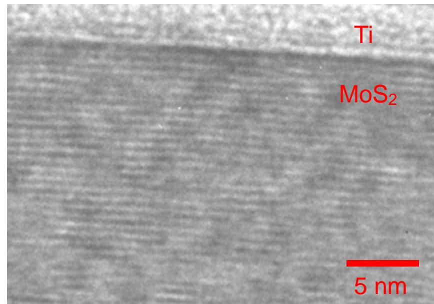

Figure S2. A cross-sectional TEM image of the interface between Ti and MoS_2 before laser annealing.

References

[1] Bonn, M.; Denzler, D. N.; Funk, S.; Wolf, M.; Wellershoff, S.-S.; Hohlfeld, J. Ultrafast electron dynamics at metal surfaces: competition between electron-phonon coupling and hot-electron transport. *Phys. Rev. B* **2000**, *61*, 1101-1105.

[2] Luther-Davies, B.; Rode, A. V.; Madsen, N. R.; Gamaly, E. G. Picosecond high-repetition-rate pulsed laser ablation of dielectrics: the effect of energy accumulation between pulses. *Opt. Eng.* **2005**, *44*, 051102

[3] Chimmalgi, A.; Grigoropoulos, C. P.; Komvopoulos, K. Surface nanostructuring by nano-/femtosecond laser-assisted scanning force microscopy. *J. Appl. Phys.* **2005**, *97*, 104319.

[4] Anisimov, S.I.; Rethfeld, B. On the theory of ultrashort laser pulse interaction with a metal. *Proc. SPIE* **1997**, *61*, 1642-1655.

[5] Kim, J. Y.; Choi, S. M.; Seo, W. S.; Cho, W. S. Thermal and electronic properties of exfoliated metal chalcogenides. *B. Korean Chem. Soc.* **2010**, *31*, 3225-3227.